Journal of Radiotherapy in Practice

cambridge.org/jrp

Radiation dose diode measurements for in vivo dosimetry of IMRT plans: accuracy and technical considerations

Ali H. Abdelkader, Ali M. AlZein and Bilal H. Shahine

Department of Radiation Oncology, American University of Beirut Medical Center, Beirut, Lebanon

Original Article

Cite this article: Abdelkader AH, AlZein AM, and Shahine BH. (2025) Radiation dose diode measurements for in vivo dosimetry of IMRT plans: accuracy and technical considerations. *Journal of Radiotherapy in Practice*. **24**(e5), 1–7. doi: 10.1017/S1460396925000020

Received: 28 May 2024
Revised: 12 December 2024
Accepted: 7 January 2025

Keywords:
Diode; Entrance radiation dose measurements; In vivo dosimetry; step-and-shoot IMRT

Corresponding author:
Bilal Shahine; Email: bs39@aub.edu.lb

Abstract

Introduction: In vivo diode dosimetry proved its efficacy as a patient-specific quality assurance tool for 3DCRT. Its usefulness in IMRT is not sufficiently investigated.
Methods: Four step-and-shoot IMRT plans were generated for different treatment sites using an Alderson Rando anthropomorphic phantom. Two in vivo semiconductor diodes were used to perform 33 entrance radiation dose measurements at central axis and max beam point dose on a water-equivalent slabs based on the anthropomorphic plans. Measured values were compared to planned ones, and detailed analysis per segment of each IMRT field was made to infer the reason behind the discrepancies of measurements from expectations.
Results: Point dose measurements were performed on a beam and a segment basis. Agreement within ±5% action level with planned dose was 27% of beams at central axis versus 45% at max point dose and 10% of segments at central axis versus 25% at max point dose. For ±10% action level, 70% of beams at central axis versus 73% at max point dose, and 15% of segments at central axis versus 41% at max point dose. Classification of segments resulted in a significance of .021 for measuring at positions unaffected by the MLC partial and total blockage.
Conclusion: Diode measurements are recommended at maximum dose coordinates for open beams/segments for more accurate patient dose verification results as part of in vivo dosimetry. This is important for limited resources centres treating with sMLC IMRT.

Introduction

Point-measuring radiation detectors have been widely used in radiotherapy for a long time for absolute and relative, in addition to in-phantom and in vivo dose measurements whether in or outside the radiation field. Measuring the dose with the emerging complex radiotherapy techniques that aim at safe and efficient delivery to patients is difficult and vital at the same time.[1] The French National Cancer Institute (INCa) authorization criteria for external radiotherapy practice require performing in vivo dosimetry (IVD) for each technically measurable beam during the first or second treatment session and when modification of treatment is introduced.

Ex vivo or in vitro dose measurements are made before the treatment on a phantom representing the patient. However, IVD is the measurement of the radiation dose absorbed by the patient's body while receiving treatment to confirm that the treatment is delivered as planned.[2–4] It only includes the measurements done during patient treatment which provide quantitative data of the actual dose delivered to the patient.[1] IVD aims at detecting major treatment errors, recording the dose delivered to patients, alerting for deviations of delivered dose from the planned one, and fulfilling legal requirements if applied.[1–3] In addition, it keeps tracking the dose delivered during radiotherapy to the patient rather than the individual components prior to treatment in other quality assurance (QA) methods.[5] Also, IVD judges the treatment session by checking the absorbed dose that has been delivered to the patient through the dosimeters placed on the skin or in natural cavities of the patient and traces detected deviations to figure out the faulty step behind it.[6]

During external beam radiation therapy (EBRT), a point dosimeter is placed on the skin of a patient at the beam entrance side to perform entrance radiation dose measurements.[1,5,6] These surface measurements are used to infer the dose absorbed by an interest point inside the patient that in turn is compared with its equivalent on the treatment planning system (TPS).[5] The relationship between doses at different sites enables to relate the detector response to the dose inside the patient.[3] Clinical action is taken when measurements diverge from expectations beyond the tolerance levels.[5]

Intensity-modulated radiation therapy (IMRT) is a new type of radiation therapy that uses advanced technology in manipulating intensities of multiple radiation beams to precisely irradiate and treat a tumour. Beam modulation at fixed gantry and collimator angles is obtained with the help of multi-leaf collimators (MLCs). The intensity-modulated fields can be delivered

either by static MLC (sMLC) mode or by dynamic MLC (dMLC) mode. The former involves radiation delivery when MLCs are stationary (step-and-shoot delivery), whereas the latter encompasses radiation delivery when MLCs are moving (sliding window delivery).[7,8]

Most radiotherapy departments and centres are shifting from conventional techniques into modern ones, for instance electronic portal imaging device transmission dosimetry, but many fall behind due to lack of resources. IVD is the only QA method which is considered sensitive to the actual patient setup. Diode IVD gives real-time readout measurements during the actual treatment. Hence, it may be superior to pretreatment verification tools used for routine IMRT QA. Diode IVD measurements may be prone to large uncertainties because of high gradient dose regions.[9–11]. It is often abandoned performing IVD on IMRT patients because of the questionable accuracy in the presence of many dose gradients within IMRT treatment fields.[10] Diodes link the detailed phantom measurements to the treatment situation, as IVD adds a necessary IMRT QA component.[12] Diode IVD is faster, gives instant readouts as opposed to routine IMRT QA pretreatment verification tools, and does not require additional equipment from what is already used for conventional treatment techniques.[9,11]

A few researchers investigated the delivered dose accuracy on IMRT plans with diode dosimetry.[9–13] Kadesjö, et al.[9] and Vinall, et al.[10] suitably positioned diodes based on the energy fluence distribution, as IVD measurements are highly position dependent. Point measurements were taken five millimetres at least from any high-dose gradients to get accurate results.[9,11] The central axes of the fields were the preferred diode positioning choice, along which expected doses were extracted from single depth of dose maximum (d_{max}) point measurements, to reduce positioning uncertainties.[11,12] A trend was found in diode response with respect to the target size. The response of the diode was higher with larger target sizes, which had larger segments. The increase in segment sizes increased the scatter dose reaching the dosimeters. Also, partial blockage of the diode by the MLCs affected its response; however, the corresponding patient measurements were performed at central axis.[13] The current work aims to perform ex vivo radiation dose measurements with diode dosimeters for brain, breast, lung and prostate treatment sites on an anthropomorphic phantom to assess measurement accuracy on the levels of beams and segments and to evaluate the overall feasibility of performing diode-based IVD as a routine QA procedure in sMLC IMRT. Two locations for the diode placement were chosen, one at the standard central axis and the other at maximum dose point for future adoption. This work sheds light on the importance of conducting further research and updating IVD regulations for advanced treatment techniques. This is worthy especially for limited resource centres in developing countries delivering sMLC IMRT treatment and performing diode patient-specific QA. The investigation was conducted at the Department of Radiation Oncology, American University of Beirut Medical Center.

Methods

Calibration

Two p-type silicon in vivo semiconductor probes T60010M (PTW-Freiburg, Freiburg, Germany) connected to the MULTIDOS electrometer T10004 (PTW-Freiburg, Freiburg, Germany) through the MULTIDOS TBI BOX T16009 (PTW-Freiburg, Freiburg, Germany) were calibrated for measuring entrance dose. Both diodes have a 2·0 g/cm^2 build-up cap of lead for the 5-13 MV photon energy range and an effective detection volume of 1 mm^2 circular area and 2·5 μm thickness. A Farmer ionization chamber TM30013 (PTW-Freiburg, Freiburg, Germany) connected to the PTW UNIDOS electrometer was used as the reference detector for calibration.

Diodes, mounted on a thin plate and surrounded by a flat/hemispherical build-up cap, were embedded in a foam piece to easily fasten and handle them. The standard irradiation conditions used were a field size of 10x10 cm^2, a 100 cm SSD, a 0° angle and 200 monitor units equivalent to approximately 200 cGy at maximum dose depth. At the time of calibration, temperature and pressure were 24°C and 100.3 kPa.

Diodes were individually calibrated against the ionization chamber for photon irradiation of 6 MV energy using a Siemens Artiste linear accelerator (Siemens, Munich, Germany). The semiconductor diodes were placed on the front surface of a 5·5 cm thick water-equivalent phantom two centimetres from the beam central axis to avoid shadowing with the ionization chamber that was placed at d_{max} (1·5 cm) at the beam central axis. Then, the signal of each diode was compared to the absorbed dose determined with the ionization chamber according to IAEA TRS398 code of practice.[14]

The entrance calibration factor, $F_{entrance}$, is the quotient of the entrance dose in d_{max} measured with the chamber, $D_{entrance}$, by the entrance dose measured with probe, $M_{entrance}$:[14]

$$\boldsymbol{F}_{entrance} = \boldsymbol{D}_{entrance}/\boldsymbol{M}_{entrance} \quad (1)$$

$D_{entrance}$ was obtained by multiplying the entrance reading of the chamber with the ionization chamber calibration coefficient ($N_{cal} = 5{\cdot}393\text{x}10^7$ Gy/C) and the temperature and pressure correction factor:[14]

$$\boldsymbol{D} = \boldsymbol{M}\boldsymbol{N}_{cal}\boldsymbol{k}_{QQ_o}\boldsymbol{k}_{TP} \quad (2)$$

where k_{QQo} is the beam quality correction factor. Output is 1 cGy/MU set at 100 SSD.

Treatment planning

Eclipse TPS version 15·1 (Varian Medical Systems, Palo Alto, USA) was used to create brain, breast, lung and prostate sMLC IMRT plans on the CT scan of the anthropomorphic phantom. AAA (Analytical Anisotropic Algorithm) was the used calculation model. The plans were transferred to the R&V system MOSAIQ (Elekta AB, Stockholm, Sweden) and delivered using the Siemens Artiste linear accelerator (Siemens, Munich, Germany) of 160-leaf MLCs with 6 MV photons.

1. The Brain Plan—The prescription was 250 cGy per fraction. The brain was contoured on the scan of the anthropomorphic phantom for cranial irradiation with hippocampal sparing. The hippocampus was contoured, and the hippocampal avoidance region was generated by expanding the hippocampal contour by 5 mm volumetrically. Figure 1a shows nine coplanar fields all around the head at a 40° equal spacing from 20° to 340°.

2. The Left Breast Plan—A dose of 200 cGy per fraction was prescribed. Figure 1b shows the seven equally spaced fields generated on a gantry angle range of 180° from 330° to 150° around the left breast with the isocentre fixed at the centre of PTV mass.

https://doi.org/10.1017/S1460396925000020 Published online by Cambridge University Press

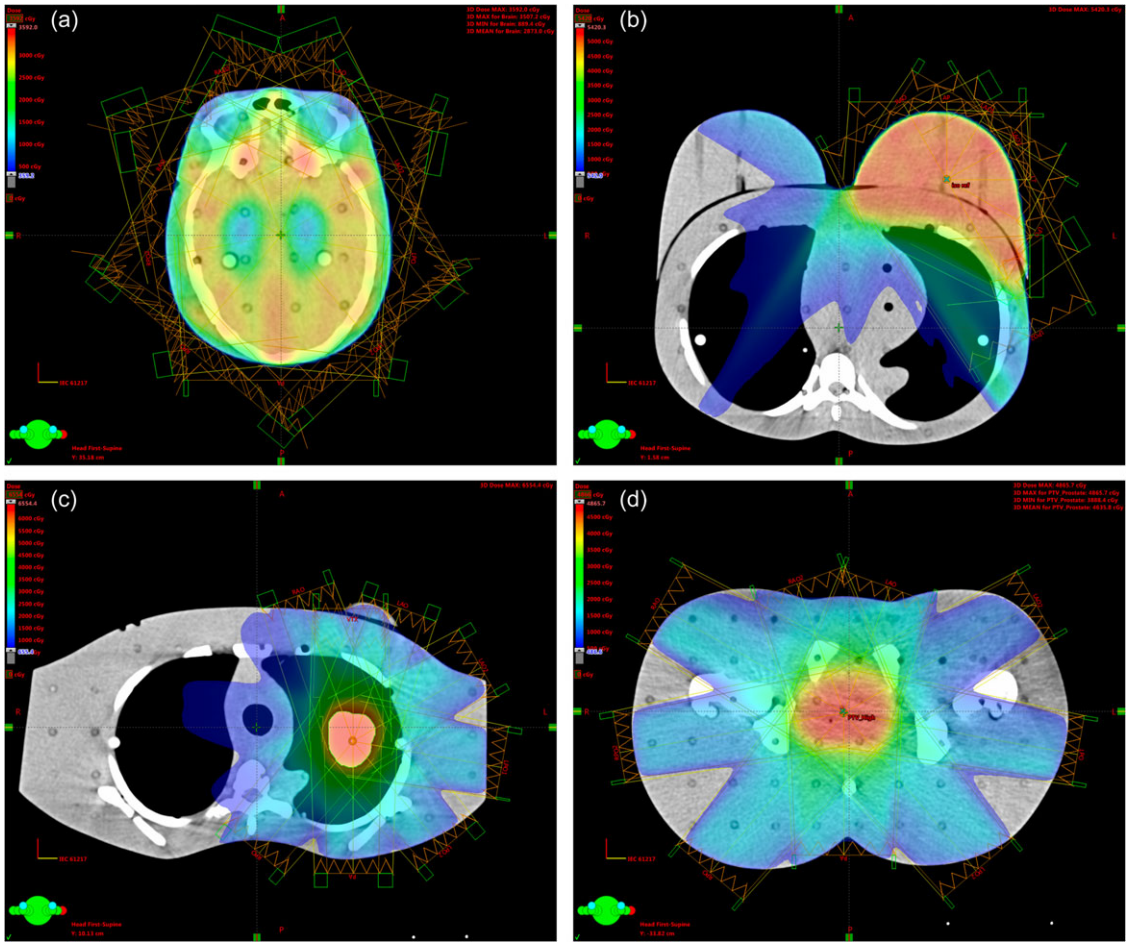

Figure 1. The axial plane of the anthropomorphic phantom scan for the four treatment plans: (a) brain, (b) left breast, (c) left lung, and (d) prostate.

The setup has two opposing fields, as most of the dose is normally applied through tangents. Collimator was kept at 0° for all fields, and beams are coplanar.

3. The Left Lung Plan—The prescription was 200 cGy per fraction. Figure 1c shows eight fields surrounding the left side of the phantom including a non-coplanar field arrangement. The seven other fields have a 40° equal spacing angle from 20° to 340° and a zero-degree collimator rotation.

4. The Prostate Plan—For the pelvic site, 200 cGy per fraction was prescribed. Prostate was contoured and surrounded with a PTV. Organs at risk, bladder, rectum and femoral heads, were also contoured. Figure 1d shows the nine equally spaced fields generated in external beam planning all around the anthropomorphic phantom, whose couch rotation angle was set to zero degrees. However, the collimator rotation of five fields was set to 90°.

QA verification plans were created for all four treatment plans. Gantry and couch were reset to zero degrees. Each field was placed into a separate verification plan with only one fraction. The planned dose at d_{max}, 1·5 cm for 6 MV photon beams, was extracted from the treatment plan for each field. Planned dose at the central axis and dose max along with its coordinates were recorded and all values were tabulated in a Microsoft Excel spreadsheet.

Moreover, step-and-shoot delivery enabled obtaining cumulative dose reference coefficients (CDRC) of central axis and dose max reference points at d_{max} from the Digital Imaging and Communications in Medicine (DICOM) Validation Toolkit (DVTk) (ICT Healthcare, Eindhoven, The Netherlands) for each control point in all beams. These coefficients were used to calculate the dose reference coefficients (DRC),

$$DRC_i = CRC_j - CDRC_{j-1} \tag{3}$$

where i = (j+1)/2 and j is an odd natural number, and the expected dose per segment in all beams:

$$D_i = DRC_i \times prescription \tag{4}$$

Furthermore, max dose and central axis measurement positions in each segment were categorized into totally blocked (TB), partially blocked (PB) and open (O). Figure 2a and b shows two segments as an example of total and partial blockage of the measurement point by the MLCs, where a circle of radius 0.1 cm (least possible value on the TPS) was used to represent the effective detection area of the used diodes (radius ~ 0·6 mm).

Point dose measurements

Radiation dose measurements were taken for every field in each plan. A 17·5 cm thick water-equivalent phantom (slabs) was used instead of the Alderson Rando phantom to eliminate the effect of directional dependence and positioning errors due to its curves.

https://doi.org/10.1017/S1460396925000020 Published online by Cambridge University Press

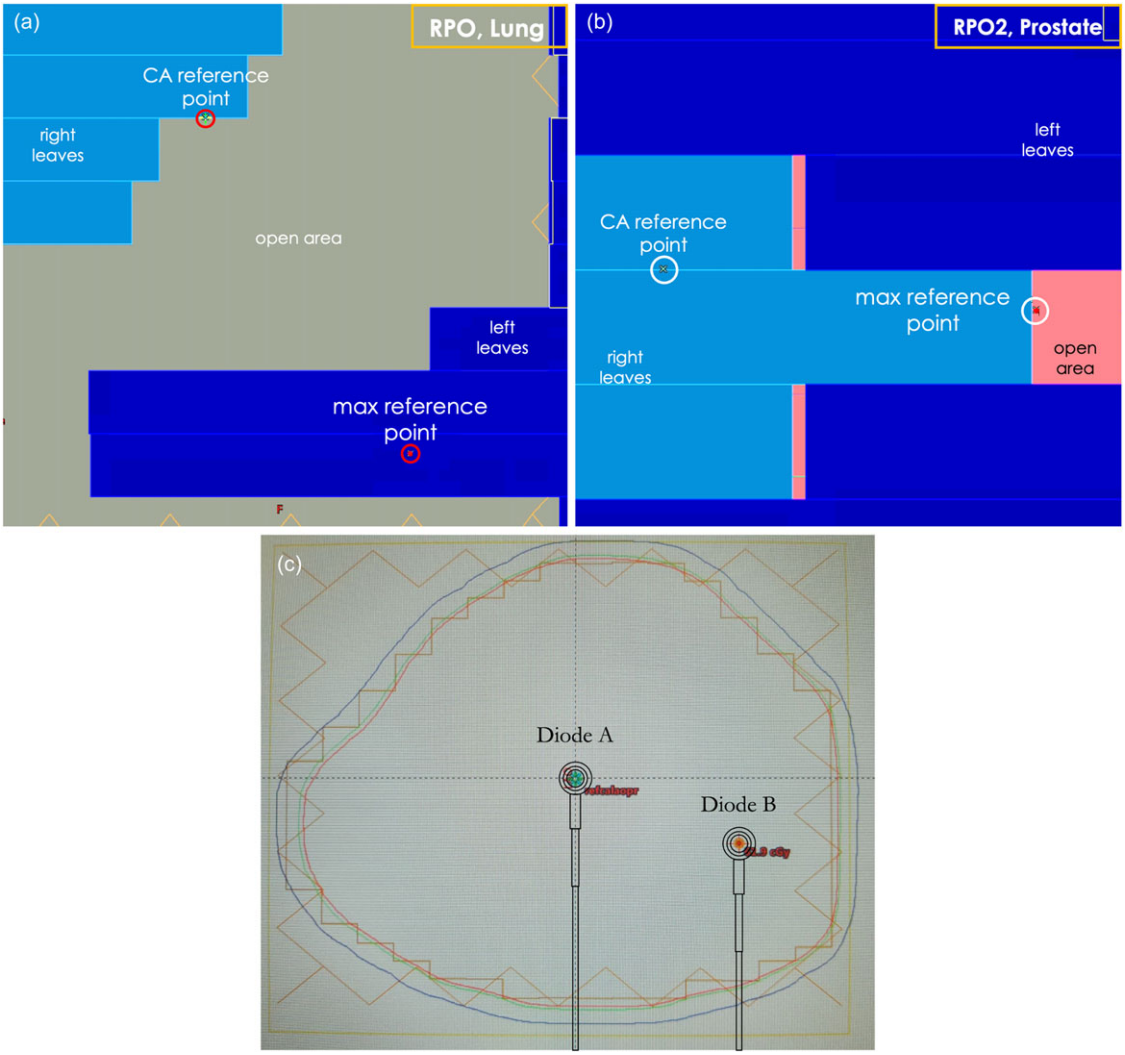

Figure 2. MLCs totally and partially blocking the max dose and central axis measurement points in segments 5 and 7 of beams (a) 'RPO' and (b) 'RPO2' in the left lung and prostate cases, respectively. (c) The central axis and max dose positions at which diodes A and B are placed, respectively, in the 'LAO' beam of the prostate plan.

Beams were delivered individually with the same reference settings of calibration.

Diode A was positioned at the central axis (0, 0) in all measurements, while diode B position was changed for every beam based on the maximum dose coordinates (x, y). For that purpose, a graph paper with the coordinates was used to easily change the position of diode B for each beam in every plan. Our graph paper was 1 millimetre scale, so diode positional accuracy or error estimate can be taken as half of the scale width amounting to 0·5 mm. In clinical practice, the graph paper tool can be easily adopted to position the diode on curved surfaces and maintain its positional accuracy.

Figure 2c shows the positioning of diode A at the origin and diode B at the dose max coordinates of beam 'LAO' from the prostate case. The MULTIDOS electrometer and the MULTIDOS TBI BOX used in calibration were also used for measurements.

Measurements were made for every single beam in the same way. The diodes readings were tabulated in the excel sheet. Also, video recordings were made during irradiation to extract readings of the diodes segment by segment for each beam. Entrance doses at central axis and at dose max coordinates were calculated by multiplying the measured readings of diodes A and B (M_A & M_B) by their corresponding entrance calibration factor (F_A & F_B):[14]

$$\boldsymbol{D}_{entrance} = \boldsymbol{MF}_{entrance} \quad (5)$$

Percentage difference (Δ) between measured entrance dose (D) and planned TPS dose (D_{TPS}) at d_{max} (Central Axis and Max Dose Point) was calculated to evaluate deviation from expected dose according to the equation:[13]

$$\boldsymbol{\Delta} = \boldsymbol{100}(\boldsymbol{D} - \boldsymbol{D}_{TPS})/\boldsymbol{D}_{TPS} \quad (6)$$

To examine the difference between results, Student's t-test statistic operation was performed. The significance threshold was set at 0·05.

Results

The entrance calibration factors of diodes A and B, F_A and F_B, are 0·5300 and 0·5384 cGy/nC, respectively.

Table 1 lists the maximum dose D_{MDP}, its coordinates (x, y), and the central axis dose D_{CA} for all nine fields of the prostate

https://doi.org/10.1017/S1460396925000020 Published online by Cambridge University Press

Table 1. The expected and measured doses along with their corresponding percentage differences at both positions for all prostate beams and segments of the LPO beam

		MDP coordinates		D_{MDP} (cGy)			D_{CA} (cGy)		
Site	Field	x (cm)	y (cm)	Expected	Measured	Δ_{MDP} (%)	Expected	Measured	Δ_{CA} (%)
Prostate 9 fields	LAO	1·9	−0·8	61·9	57·8	−6·7	56·1	52.1	−7·1
	LAO2	−0·7	−0·5	42·5	39·8	−6·3	39·1	37.6	−3·8
	LPO	1·4	0·2	60·8	59·6	−2·0	50·1	44·8	−10·6
	LPO2	−0·4	1·4	59·7	57·0	−4·6	53·5	50·4	−5·8
	PA	2·1	−0·2	51·5	48·5	−5·8	37·8	34·7	−8·2
	RPO	−0·2	1·7	63·8	61·9	−2·9	59·7	56·2	−5·8
	RPO2	1·4	−0·1	56·8	52·8	−7·0	56	52·0	−7·2
	RAO	−1·4	1·4	73	71·3	−2·3	60·9	56·4	−7·3
	RAO2	0·9	−1·1	33·9	31·7	−6·5	33·7	31·9	−5·5
Field					**LPO—Prostate**				
Segment @ CA		1: O	2: O	3: O	4: O	5: O	6: PB	7: TB	
$D_{CA,\ m}$ (cGy)		7·0	10·8	7·9	8·8	7·3	2·8	0·1	
$D_{CA,\ e}$ (cGy)		5·5	9·3	6·6	7·3	5·9	6·6	8·8	
Δ_{CA} (%)		**26·5**	**15·9**	**20·7**	**19·6**	**22·7**	**−57·1**	**−98·3**	
Segment @ MDP		1: O	2: O	3: O	4: O	5: O	6: O	7: O	
$D_{MDP,\ m}$ (cGy)		6·9	10·7	7·9	8·7	7·3	7·9	10·1	
$D_{MDP,\ e}$ (cGy)		6·7	11·3	8·0	8·9	7·2	8·0	10·7	
Δ_{MDP} (%)		**3·7**	**−5·2**	**−1·0**	**−2·1**	**0·8**	**−0·7**	**−5·1**	

Table 2. Percentage of beams and segments having measured dose within ±5% and ±10% of the expected one for the different treatment plans at the MDP and CA positions

		MDP		CA			MDP		CA	
	Beams	% < ±5%	% < ±10%	% < ±5%	% < ±10%	Segments	% < ±5%	% < ±10%	% < ±5%	% < ±10%
Brain	9	56	56	44	56	74	20	20	1	3
Breast	7	14	29	29	43	62	2	8	0	0
Lung	8	63	100	25	87	56	20	50	2	13
Prostate	9	44	100	11	89	60	58	92	37	50
All Plans	33	45	73	27	70	252	25	41	10	15

treatment plan as calculated by the TPS. It also shows the equivalent measured doses obtained with the readings of the two calibrated diodes at both measurement positions. Percentage differences of measured and calculated doses at the coordinates Δ_{MDP} and central axis Δ_{CA} are correspondingly shown. The second part of the table shows the same analysis done on the segment level for the 'LPO' beam of the prostate plan.

In addition, Table 2 presents the percentage of beams and segments for which the measured dose is within ±5% and ±10% of the expected one for the four treatment plans at both measurement positions.

The percentage of segments having the measurement points (max dose point and central axis one) O, as well as TB & PB, by the MLCs per plan are tabulated in Table 3a. For those classified as open and partially blocked, the percentage of segments having the measured dose within ±5% and ±10% of the expected dose per category are also shown for both positions in Table 3b.

The percentage of segments having open measurement points (% O) together with the mean absolute error percentage (MAE) associated with beams and segments is listed for each treatment plan at both positions in Table 4.

Discussion

The measured results obtained for the left lung and the prostate plans show lower discrepancies with expected results than those for

https://doi.org/10.1017/S1460396925000020 Published online by Cambridge University Press

Table 3. (a) Percentage of totally blocked (TB) & partially blocked (PB) and open (O) segments according to the measurement points with respect to the MLCs for each plan and (b) the percentage of PB & O segments having the measured dose within ±5% and ±10% of the expected one at both measurement positions

		MDP			CA		
(a)	Segments	**TB** (%)	**PB** (%)	**O** (%)	**TB** (%)	**PB** (%)	**O** (%)
Brain	74	28	3	69	59	26	15
Breast	62	28	3	69	66	7	27
Lung	56	5	5	90	21	16	63
Prostate	60	0	2	98	13	7	80

	PB				O			
(b)	MDP		CA		MDP		CA	
% within	**±5%**	**±10%**	**±5%**	**±10%**	**±5%**	**±10%**	**±5%**	**±10%**
Brain	1	1	1	3	19	19	0	0
Breast	0	0	0	0	2	8	0	0
Lung	2	2	0	0	18	48	2	13
Prostate	0	0	2	2	58	92	35	48

Table 4. Percentage of segments having open measurement points and the beams/segments MAE at the two examined positions for the four treatment plans

	% O		Beam MAE		Segment MAE	
	MDP	CA	MDP	CA	MDP	CA
Brain	69	15	5·7	8·3	59·8	112·4
Breast	69	27	8·4	11·2	60·1	100·9
Lung	90	63	4·7	6·5	15·9	41·9
Prostate	98	80	4·7	6·8	5·8	24·4
p value	.021		.002		.020	

the brain and left breast. Table 1 is an example of the data obtained per beam in the prostate plan and a segments analysis of the 'LPO' beam. Since the measurements at the central axis and the max dose point (MDP) were taken simultaneously, positioning diodes together caused misplacements of the diode measuring the max dose in three beams. This was due to the size of the probes. With one diode at the centre and the probes having radii of 0·6 cm, the other diode was not positioned correctly at its position (x, y) when its radial distance from the origin was less than 1·2 cm. For that, the percentage differences at max point for breast 'LAO2', Lung 'LPO2' and prostate 'LAO2' were also excluded from the MAE values. The radial distance of their max measurement point were 0·9 cm, 0·2 cm and 0·8 cm, respectively.

Table 2 shows better accuracy was achieved with the MDP measurements against the central axis ones at the level of beams analysis except for the breast plan. On the segments level, analysis has proved the supremacy of the MDP over CA in all plans. In vivo measurements should be analysed on the segments level to obtain consistency in the values. The percentage of beams having the measured dose within ±10% of the expected dose is 29% when measuring at the MDP versus 43% at the central axis in the breast plan. For segments, it increased from 0% at the central axis to 8% at the max dose position. The higher percentages obtained in beams measurements at both positions are due to the fact that errors occurring on the segments level cancel each other out in every beam (positive and negative values of the percentage differences). This certainly raises concerns about patients' safety and necessitates segment-level measurements and investigations. One can conclude that 73% of diode point measurements at maximum dose point were within 10% action level, and hence, 27% of the times measurements failed due to intrinsic device limitation and not because of treatment errors. Our results were similar to previously published data;[13] however, we provided improved data based on MDP measurements and further supported our evidence by performing segment-based analysis. These findings point out inaccuracies of diode dose measurements in clinical practice that can be minimized by adopting maximum point dose location as a measurement point.

In Table 3a, the percentage of segments being open at the MDP is higher than that at the CA point in all treatment plans. The segments having the max measurement point TB or PB are less than those of the CA point. This trend made it possible to achieve an all-beams agreement to ±10% in the left lung and prostate plans (Table 2). When inspecting the data of doses per segment for both placement positions, MLC partial and total blockage of these positions were responsible for the high discrepancies resulted per beam between the measured and expected doses. The percentages of open segments having the measured dose within ±5% and ±10% of the expected dose for both positions in Table 3b match the values related to segments in Table 2 for the various treatment plans. This means that only open measurement positions give good agreements between measured and expected doses. Measurements related to totally blocked segments had no contribution to the values within ±5% and ±10% at both positions in all plans. More complex treatment plans tend to have more peaks and valleys in their fluence maps, resulting in larger number and smaller sized segments per beam. The brain and breast plans in this study fell into the latter category of plans, and their associated diode dose measurements were mainly inaccurate within the ±5% and ±10% threshold limits.

Table 4 confirms the measurement preference at the MDP percentage of open measurement points and MAE against the central axis point. In the comparison of the measurement positions (MDP & CA), it was found that the percentage of open segments at MDP is significantly higher than that at CA ($p = .021$) and that the

https://doi.org/10.1017/S1460396925000020 Published online by Cambridge University Press

error at MDP is significantly lower than that at CA ($p = .002$ for the beams level comparison and $p = .020$ for the segments level comparison).

Thus, lower variations are obtained with the max placement position, and better results are achieved with beams of open segments at the measurement point. Also, it is worth noting that Table 4 revealed an inversely proportional relationship between the percentage of open segments and MAE and provided an evidence base for our conclusions. This comes in total agreement with previous work[13] which concluded that discrepancies were due to total or partial irradiation of the diode, and hence, we are recommending measurements at MDP for improved clinical practice.

Conclusion

IVD for IMRT using diodes should be done at measurement points that are neither partially nor totally blocked by the MLCs. This was investigated on a slab phantom to control the parameters that would affect the results. Between the measurement points, diode positioning at the max dose coordinates gave lower discrepancies than that at the central axis.

IVD can satisfy three main things: verification of the patient dose calculation, patient setup, and treatment unit performance.[10] However, when applied with diodes for IMRT technique, it has some limitations due to the high dose gradient areas, the effect of MLCs and diode positioning criteria.

The placement position of the diode combined with the effect of the MLCs affected the results of the radiation dose measurements with diodes for brain, breast, lung and prostate IMRT plans. When performing diode IVD for IMRT plans, whether as a last QA check or as a regulatory process, it is recommended to only measure open beams at the max dose coordinates while being precise in diode placement and looking out for steep dose gradients in addition to a ±10% action level. For the patient's utmost benefit, segment-level measurements turned out to be crucially significant in sMLC IMRT.

The challenge of using diode IVD for IMRT arises from positioning uncertainties in high gradient regions of the inhomogeneous fluence distribution within the beams; hence, the importance of placing measurement points away from such regions (choice of open areas). Our patient-specific QA measurements quantified the accuracy of IVD in sMLC IMRT settings, especially for centres of limited resource availability in developing countries.

Acknowledgements. We would like to thank Ibrahim Duhaini for initiating this topic and Zainab Alsayed for reviewing the manuscript.

Data availability statement. Bilal Shahine and Ali Abdelkader have full access to all the data in the study. Research data are stored in an institutional repository and will be shared upon request to the corresponding author.

Competing interests. The authors declare none.

Financial support. This research received no specific grant from any funding agency, commercial or not-for-profit sectors.

References

1. Mijnheer B. Clinical 3D Dosimetry in Modern Radiation Therapy. 1st ed. Boca Raton (Florida): CRC Press; 2017.
2. Olaciregui-Ruiz I, Beddar S, Greer P, et al. In vivo dosimetry in external beam photon radiotherapy: requirements and future directions for research, development, and clinical practice. Phys Imaging Radiat Oncol 2020; 15: 108–116. https://doi.org/10.1016/j.phro.2020.08.003.
3. Mijnheer B, Beddar S, Izewska J, Reft C. In vivo dosimetry in external beam radiotherapy. Med Phys 2013; 40: 070903. https://doi.org/10.1118/1.4811216.
4. International Atomic Energy Agency. Development of Procedures for In Vivo Dosimetry in Radiotherapy. Vienna: IAEA; 2013.
5. American Association of Physicists in Medicine. Diode In Vivo Dosimetry for Patients Receiving External Beam Radiation Therapy, Madison (Wisconsin): Medical Physics Publishing; 2005. https://doi.org/10.37206/88.
6. Van Dam J, Marinello G. Methods for In Vivo Dosimetry in External Radiotherapy. 2nd ed. Brussels: ESTRO; 2006.
7. Dieterich S, Ford E, Pavord D, Zeng J. Practical Radiation Oncology Physics. 1st ed. Philadelphia: Elsevier; 2016.
8. Khan FM, Gibbons JP. Khan's The Physics of Radiation Therapy. 5th ed. Philadelphia: Lippincott Williams & Wilkins; 2014.
9. Kadesjö N, Nyholm T, Olofsson J. A practical approach to diode based in vivo dosimetry for intensity modulated radiotherapy. Radiother Oncol 2011; 98: 378–381. https://doi.org/10.1016/j.radonc.2010.12.018.
10. Vinall AJ, Williams AJ, Currie VE, Van Esch A, Huyskens D. Practical guidelines for routine intensity modulated radiotherapy verification: pretreatment verification with portal dosimetry and treatment verification with in vivo dosimetry. Br J Radiol 2010; 83: 949–957. https://doi.org/10.1259/bjr/31573847.
11. Al-Shareef JM, Attalla EM, El-Gebaly RH, Deiab NA, Abdelmajeed M, Fathy MM. Implementation of in vivo diode dosimetry for intensity modulated radiotherapy as routine patients' quality assurance. Radiat Phys Chem 2021; 187: 109564. https://doi.org/10.1016/j.radphyschem.2021.109564.
12. Higgins PD, Alaei P, Gerbi BJ, Dusenbery KE. In vivo diode dosimetry for routine quality assurance in imrt. Med Phys 2003; 30: 3118–3123. https://doi.org/10.1118/1.1626989.
13. Alaei P, Higgins PD, Gerbi BJ. In vivo diode dosimetry for IMRT treatments generated by pinnacle treatment planning system. Med Dosim 2009; 34: 26–29. https://doi.org/10.1016/j.meddos.2008.01.002.
14. International Atomic Energy Agency. Absorbed Dose Determination in External Beam Radiotherapy - An International Code of Practice for Dosimetry Based on Standards of Absorbed Dose to Water. 1st ed. Vienna: IAEA; 2000.

https://doi.org/10.1017/S1460396925000020 Published online by Cambridge University Press